

The multifunctional mesoporous Sn–Cu–Ti catalysts for the B–V oxidation of cyclohexanone by molecular oxygen

Zhiwei Zhou¹ · Jianzong Wang¹ · Juan Qin² · Yang Yu¹ · Wenliang Wu¹

Published online: 22 August 2017
© Springer Science+Business Media, LLC 2017

Abstract The multifunctional three-component mesoporous Sn–Cu–Ti samples were successfully prepared by a facile one-pot AcHE method and characterized by XRD, N₂ sorption, ICP, FT-IR, UV–vis, SEM and TEM techniques, and their catalytic performances were carried out in the B–V oxidation of cyclohexanone by molecular oxygen. The results show that both tin and copper species can homogeneously incorporated in the crystalline framework of mesoporous anatase TiO₂, where tin species as the active sites would increase the Lewis acidity and the oxidation of benzaldehyde as pro-oxygenic agent would be promoted by the introduction of little copper species resulting in the improving catalytic performance. The prepared 15Sn–3Cu–Ti catalyst shows higher yield of ϵ -caprolactone than other catalysts and exhibits excellent catalytic stability even after repeated reaction for five times without any further treatment. The outstanding catalytic performance for Sn–Cu–Ti catalysts could offer a valuable reference for the industrial development of B–V oxidation of cyclohexanone.

Keywords Mesoporous Sn–Cu–Ti · AcHE method · Cyclohexanone · Molecular oxygen · Caprolactone

1 Introduction

The ϵ -caprolactone, as a kind of important organic chemical intermediate, can be used for preparation of ϵ -caprolactam, polycaprolactone and polycaprolactone polyol etc [1–7]. It was industrially prepared by B–V oxidation of cyclohexanone with peroxyacids, organic peroxide or hydrogen peroxide as oxidants. It has been demonstrated that some disadvantages regarding both safety issues and intrinsic instability must be of great concern because these oxidants are corrosive or explosive [8–11]. Recently, molecular oxygen, which is environmental friendly, cheaper and safer, would act as an ideal substitute to avoid the above problems [12–17].

Ordered mesoporous materials attracted extensive attention because of their high specific surface area, interpenetrated and regular mesoporous system and large pore size with narrow distributions [18–20]. However, since some ordered non-siliceous mesoporous materials such as mesoporous metal oxides and heteroatom mesoporous zeolites have been exploited in the latest few years [21, 22], they have been widely used as catalysts in many industrial applications. Mesoporous TiO₂ is an excellent candidate owing to its outstanding features such as being environmental friendly, excellent chemical thermal stability, as well as excellent electronic and optical properties [23–25]. However, the heteroatom species would be difficult to be incorporated into the framework of mesoporous TiO₂ because there was no active oxygen species resulting in lower interaction between the heteroatom species and the mesoporous TiO₂ [26, 27]. Therefore, the tetravalent tin (Sn⁴⁺) incorporated into the mesoporous TiO₂ would be hardly realized. In our previous study [28, 29], Sn–Ti catalysts can be successfully prepared by EISA method, and the catalytic performance can be promoted in the B–V oxidation of cyclohexanone by molecular oxygen because of its increasing Lewis acid sites

✉ Wenliang Wu
wwl@njtech.edu.cn

Juan Qin
qinjuan_1981@163.com

¹ College of Chemical Engineering, Nanjing Tech University, Nanjing 210009, People's Republic of China

² Technology and Finance Service Center of Jiangsu Province, Productivity Center of Jiangsu Province, Nanjing 210042, People's Republic of China

resulting in the activation for the carbonyl in the molecular structure of the cyclohexanone compared to mesoporous TiO_2 catalyst, which also further demonstrated that the mesoporous composite metal oxides shows higher catalytic performance.

Copper based materials [15, 30–33] have been proved to act as highly active catalysts for many oxidation reactions, especially in the oxidation of benzaldehyde, which is the co-oxidant in the B–V oxidation of cyclohexanone by molecular oxygen. Thus, the introduction of copper species in the tin based catalysts must show good catalytic performance because it can accelerate the first step of the B–V oxidation in terms of the proposed mechanism. The Fe_3O_4 -L-dopa-Cu^{II}/Sn^{IV}@m, m-SiO₂ sample shows good catalytic performance in the B–V oxidation of cyclohexanone by air in the presence of 1,2-dichloroethane as the solvent, where conversion of cyclohexanone more than 99.9% as well as selectivity of ϵ -caprolactone more than 99.9% can be obtained [34]. However, the preparation procedure of these catalysts was complicated resulting in the uncontrolled properties of these samples as well as the solvent with high toxicity. Therefore, it is essential to explore a simple and controllable method for tin and copper species doped catalysts with high catalytic performance for the B–V oxidation of cyclohexanone. However, there was no literature about the preparation for the mesoporous Sn–Cu–Ti materials for the B–V oxidation of cyclohexanone by molecular oxygen.

In this paper, a series of ordered multifunctional three-component mesoporous Sn–Cu–Ti samples with different tin and copper species loadings were synthesized by a facile one-pot AcHE method, and their chemical physical properties were also investigated by different techniques. Furthermore, the catalytic performance of these prepared samples was studied in the B–V oxidation of cyclohexanone by molecular oxygen.

2 Experimental

2.1 Sample preparation

Ordered multifunctional three-component mesoporous Sn–Cu–Ti samples were prepared in the presence of F127 as soft template according to the literature [29, 35–37]. In a typical synthesis process, 1.6 g of F127 was dissolved in 30 g anhydrous ethanol solution containing 1.4 g of hydrochloric acid and 0.6 g of acetic acid. After that, 3 g of titanium isopropoxide, a required amount of tin tetrachloride (0.09, 0.19, 0.29 and 0.38 g) and copper nitrate (0.03, 0.05, 0.07, 0.10, 0.12 g) were simultaneously added into the above solution. After being vigorously stirred at 303 K for 24 h, the resultant mixture was transferred to a Petri dish by solvent evaporation at 318 K for 48 h, and then the film

was thermally treated at 373 K for another 24 h. The final product was calcined at 623 K in air for 5 h and defined as $x\text{Sn}-y\text{Cu}-\text{Ti}$, where x and y stand for the weight percent of tin and copper species, respectively.

At the same time, the 15Sn–3Cu/Ti sample was prepared by impregnation method for comparison. 0.29 g of tin tetrachloride and 0.07 g copper nitrate was simultaneously added into the 30 g deionized water containing 0.85 g pre-synthesized mesoporous TiO_2 by AcHE method. After being stirred for 24 h, the mixture was heated to 393 K for evaporating the solvent and then dried at 373 K for another 24 h followed by calcination at 623 K in air for 5 h.

2.2 Sample characterization

XRD patterns of the samples were obtained on a Bruker D8 instrument with Ni-filtered Cu K α radiation ($\lambda = 0.154$ nm) operated at 40 kV and 30 mA. The scanning rate was $0.05^\circ \text{ s}^{-1}$ in the 2θ range from 0.75° to 80° . N_2 sorption isotherms were measured at 77 K using a Micromeritics Tristar 3000 system. The surface area was calculated by the BET method and the mesoporous size distribution was obtained by using the BJH adsorption model. The weight percent of tin and copper species was analyzed by ICP (Optima2100DV, PerkinElmer) after the sample was dissolved in HF solution. UV–vis DRS measurement was conducted on Lambda 950 spectro analysis instrument. The wavelength range was from 200 to 800 nm in the presence of BaSO_4 as reference compound. FT-IR spectra of pyridine-adsorbed were obtained on the Thermo Nicolet NEXUS spectrometer in KBr pellets. The sample was pretreated in 10^{-2} Pa at 573 K for 3 h and then cooled down to room temperature. After that, pyridine was adsorbed for 2 h and the temperature was raised to 473 K for 1 h in order to remove the physisorbed pyridine. IR spectra were measured at room temperature. The sample was dispersed in ethanol assisted by an ultrasonic technique and its morphology was visualized using a TEM (JEOL JEM 2100) operated at 120 kV. The dispersion of the semiquantitative elemental composition (Sn, Ti and O) was verified by EDX spectrometer analysis.

2.3 B–V oxidation of cyclohexanone

The B–V oxidation of cyclohexanone was performed in a three-neck flat bottom flask, where one neck was equipped with a reflux condenser and oxygen as oxidant was continuously introduced through another neck. In a typical process, 0.14 g catalyst was added into 0.5 g cyclohexanone using acetonitrile as solvent and benzaldehyde as pro-oxygenic agent, and the mixture was kept at 343 K for 5 h with continuous stirring. Then the reaction mixture was cooled down to room temperature and the product after centrifugation for removing the catalyst was analyzed on

a SP-6890 gas chromatograph equipped with a SE-30 column (0.25 $\mu\text{m} \times 50$ m). The conversion of cyclohexanone and the selectivity of ϵ -caprolactone were calculated by internal standard method using dodecane. The reusability for the catalyst was investigated by filtration without any further treatment in the next run.

3 Results and discussion

3.1 Sample characterization

XRD patterns for Sn–Cu–Ti samples with different copper species loadings are shown in Fig. 1. It can be seen from Fig. 1a that a resolved diffraction peak centered

approximately at 1.2° assigned to the (100) reflection would be observed for all the five samples, whose intensity would be promoted and shifted to higher level when the weight percent of copper species increases from 1 to 3, suggesting their ordered mesoporous structure and the decreasing interplanar spacing on the basis of the Bragg equation owing to the smaller d -spacing of CuO (0.170 nm) than it of TiO₂ (0.346 nm) probably [38, 39]. On the contrary, its intensity would decrease and it would be shifted to the lower angle with the further increase of the weight percent of copper species from 4 to 5 because of the destruction and blockage of partial pores by excessive copper species probably. As seen from Fig. 1b, the typical anatase TiO₂ structure was formed and its relative crystallinity increased when the weight percent of copper species was less than 3. However,

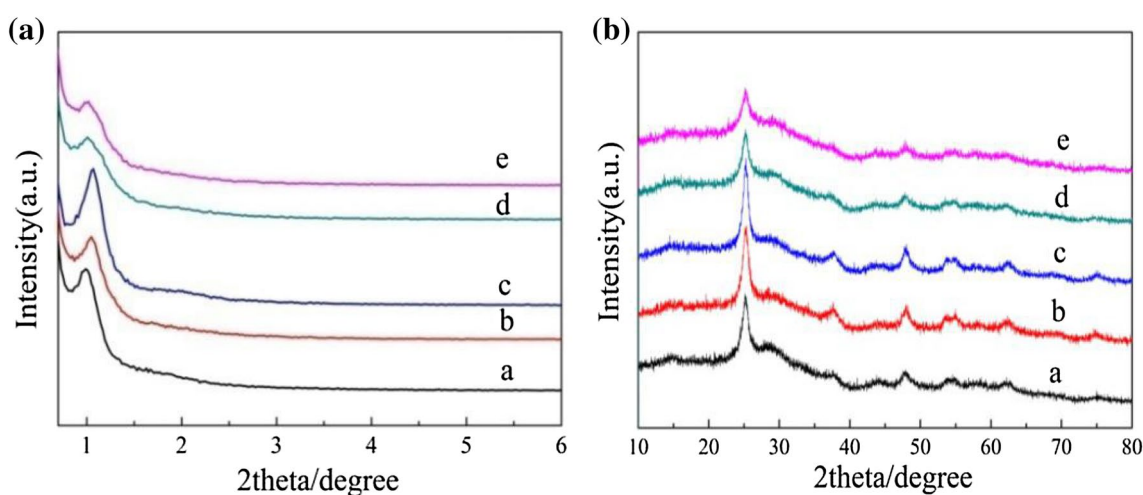


Fig. 1 Small-angle (a) and wide-angle (b) XRD patterns for Sn–Cu–Ti samples. (a) 10Sn–1Cu–Ti, (b) 10Sn–2Cu–Ti, (c) 10Sn–3Cu–Ti, (d) 10Sn–4Cu–Ti, (e) 10Sn–5Cu–Ti

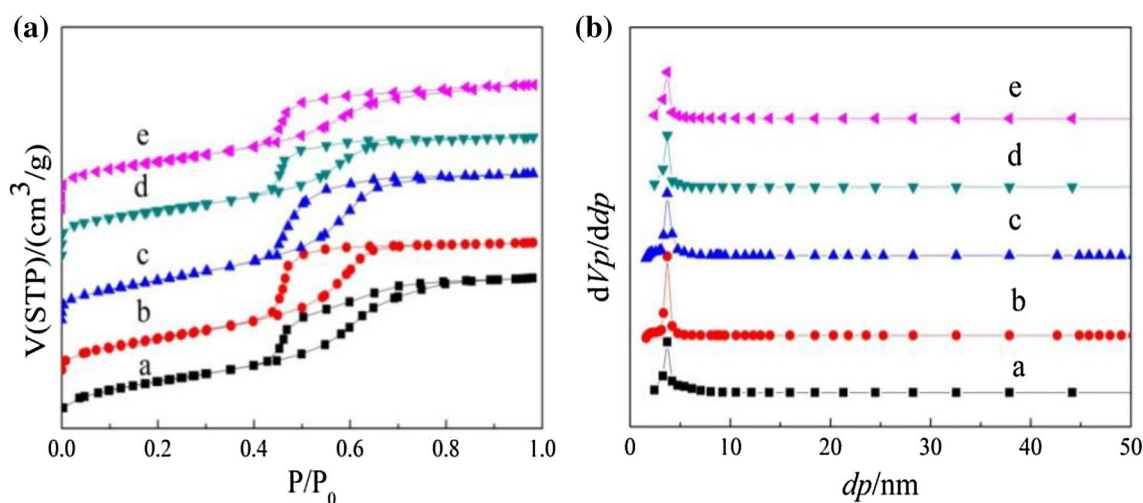


Fig. 2 N₂ sorption isotherms (a) and pore size distributions (b) for Sn–Cu–Ti samples. (a) 10Sn–1Cu–Ti, (b) 10Sn–2Cu–Ti, (c) 10Sn–3Cu–Ti, (d) 10Sn–4Cu–Ti, (e) 10Sn–5Cu–Ti

further increasing of copper species would be unfavorable. There were no any peaks corresponding to tin and copper species indicating their highly dispersion.

The N_2 sorption isotherms and pore size distributions for Sn–Cu–Ti samples are presented in Fig. 2. All the samples exhibited typical IV isotherms and sharp capillary condensation steps at the P/P_0 of 0.4–0.8, suggesting the cylindrical mesopores. At the same time, the hysteresis loop was slightly shifted to lower relative pressure and the adsorption capacity increased when the weight percent of copper species increased from 1 to 3, showing the promoting pore size from 4.7 to 5.2 nm and volume from 0.17 to 0.22 cm^3/g because of smaller atomic radius of copper (117 pm) than it of titanium (132 pm) by the incorporation of some copper

species into the framework of mesoporous TiO_2 probably even if the interplanar spacing became smaller [40, 41]. With the further increasing of copper species, the adsorption capacity decreased, which is coincident with the results of the XRD patterns. The physical properties for different Sn–Cu–Ti samples are shown in Table 1. It can be seen that surface area 183.7 m^2/g , pore size 5.2 nm and volume 0.22 cm^3/g for 10Sn–3Cu–Ti sample was higher than other samples.

The third component introduced into the EISA or AcHE system would affect severely the tremendous diversities of physical chemical properties for the prepared catalysts because the AcHE procedure was complicated and difficultly controllable. Therefore, the Sn–3Cu–Ti samples with

Table 1 Physical properties for different samples

Samples	Pore size (nm) ^a	S_{BET} (m^2/g) ^b	Pore volume (cm^3/g) ^c	Cu loading (wt%) ^d	Sn loading (wt%) ^d
10Sn–1Cu–Ti	4.7	164.0	0.17	0.83	10.08
10Sn–2Cu–Ti	5.0	173.1	0.18	1.91	9.94
10Sn–3Cu–Ti	5.2	183.7	0.22	2.86	9.97
10Sn–4Cu–Ti	5.0	167.1	0.20	3.89	9.93
10Sn–5Cu–Ti	4.9	155.5	0.19	4.81	9.96
5Sn–3Cu–Ti	5.5	160.3	0.21	2.87	4.98
15Sn–3Cu–Ti	5.0	188.1	0.26	2.95	14.94
20Sn–3Cu–Ti	4.8	174.7	0.17	2.98	19.93
15Sn–3Cu/Ti	5.7	95.7	0.32	2.89	14.81

^aBJH method

^bBET specific areas

^c $P/P_0=0.99$

^dICP-OES

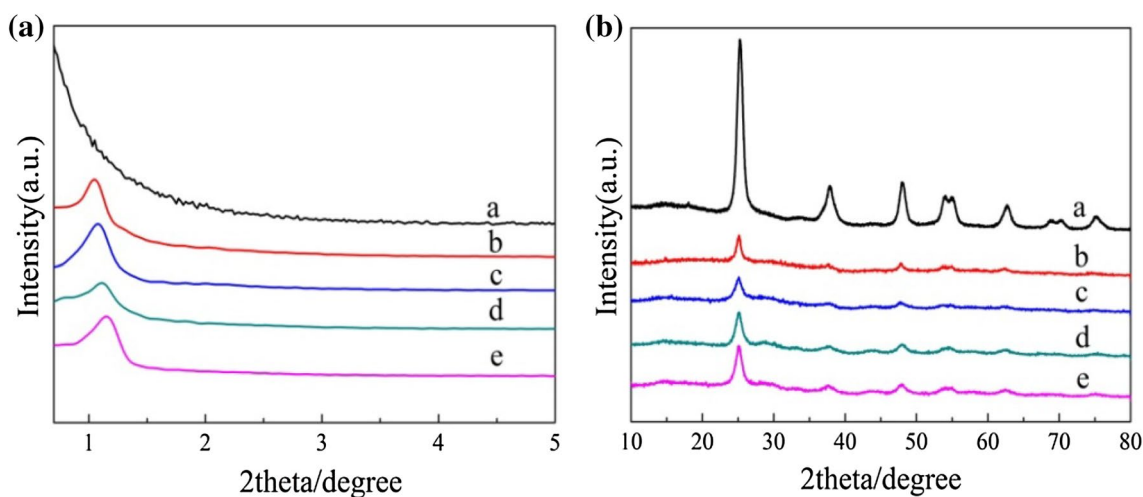


Fig. 3 Small-angle (a) and wide-angle (b) XRD patterns for different samples. (a) 15Sn–3Cu/Ti, (b) 5Sn–3Cu–Ti, (c) 10Sn–3Cu–Ti, (d) 15Sn–3Cu–Ti, (e) 20Sn–3Cu–Ti

different weight percent of tin species from 5 to 20 were prepared when the optimal weight percent of copper species was as high as 3%, and the XRD patterns are shown in Fig. 3. All the samples prepared by AcHE method exhibited an intensive diffraction peak centered at around 1.2° , indicating their ordered mesoporous structure. In addition, the peak was slightly shifted to higher level with the weight percent increasing of tin species from 5 to 20, suggesting the decreasing interplanar spacing on the basis of the Bragg equation owing to the smaller d -spacing of SnO_2 (0.211 nm) probably [42]. On the contrary, no any peak can be observed for 15Sn–3Cu/Ti sample prepared by impregnation method because of the destruction of the mesoporous framework of TiO_2 . It can be seen from Fig. 3b that the Sn–Cu–Ti samples show atypical anatase tetragonal crystal structure and its grainsize is about 12.4 nm calculated by the Scherrer equation, which is much smaller than that of commercial TiO_2 . Any peaks corresponding to tin species and copper species would not be observed, suggesting their highly dispersion.

Their N_2 sorption isotherms and corresponding pore size distributions for different samples are presented in Fig. 4. It can be seen that the isotherms of the samples are typical IV curves, which is the character for mesoporous solid materials with cylindrical channels. As seen from Fig. 4b, the narrow pore size distribution in the range of 4–5 nm for all the samples can be obtained regardless of the weight percent of tin species. Their physical chemical properties are listed in Table 1. It can be seen that the pore size would be dropped with the tin species loading increasing from 5 to 20 owing to the bigger atomic radius of tin (140 pm) as well as partial blockage of pores even when the weight percent of tin species is as high as 5%, which is excessive for its incorporation into the mesoporous framework of anatase TiO_2 probably. The specific surface area and pore volume for 15Sn–3Cu–Ti

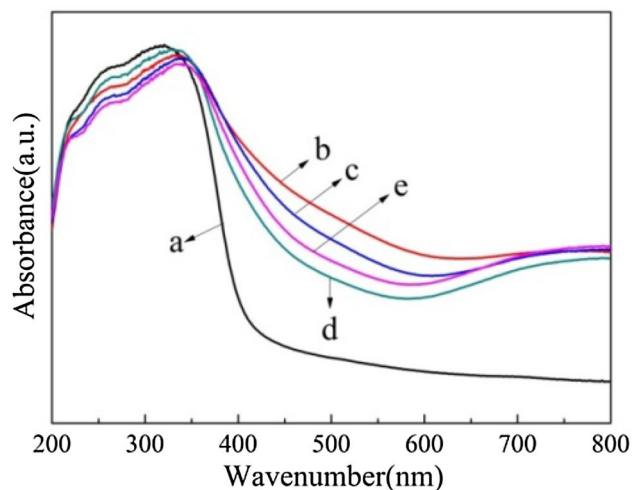


Fig. 5 UV–vis spectra for Sn–Cu–Ti samples. (a) M– TiO_2 , (b) 5Sn–3Cu–Ti, (c) 10Sn–3Cu–Ti, (d) 15Sn–3Cu–Ti, (e) 20Sn–3Cu–Ti

sample was higher than other samples. In addition, all the tin and copper species can be incorporated into the framework of TiO_2 because the actual loading of tin and copper species was found to be agreed with the theoretical value based on the ICP results.

Figure 5 shows the UV–vis spectra for different Sn–Cu–Ti samples. All the samples exhibited intensive absorption band centered at around 210 nm, suggesting ligand-to-metal charge transfer between oxygen ligand and isolated divalent tin ion (LMCT) [43]. Furthermore, compared to M– TiO_2 sample, a red shift of absorption bands can be observed owing to the reduced crystallinity [28]. A new weak and broad absorption band between 600 and 800 nm can be observed, which was generally assigned to the d – d transition

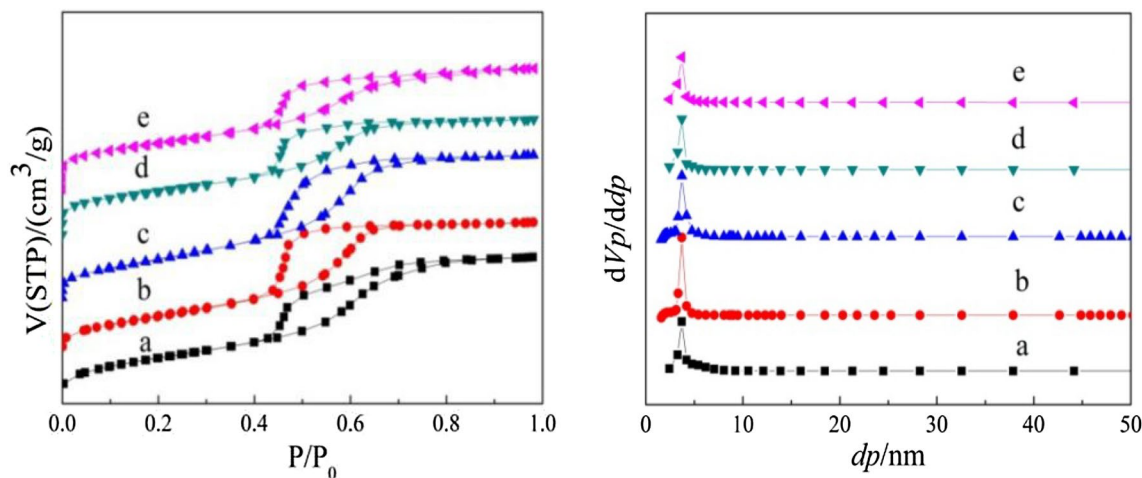


Fig. 4 N_2 sorption isotherms (a) and pore size distributions (b) for different samples. (a) 15Sn–3Cu/Ti, (b) 5Sn–3Cu–Ti, (c) 10Sn–3Cu–Ti, (d) 15Sn–3Cu–Ti, (e) 20Sn–3Cu–Ti

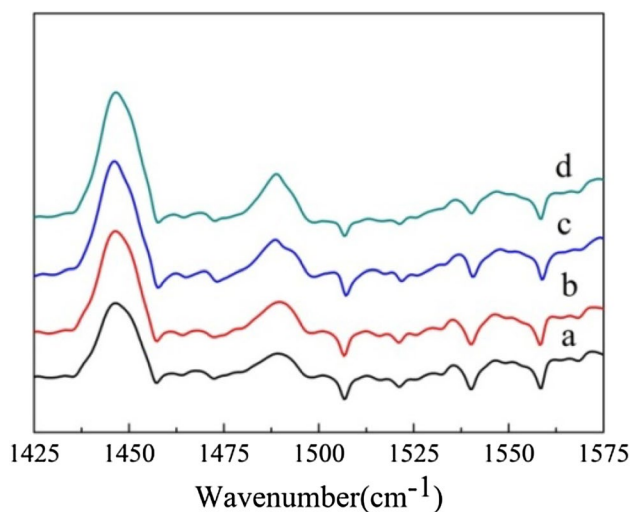


Fig. 6 FT-IR spectra of pyridine-adsorbed for Sn–Cu–Ti samples. (a) 5Sn–3Cu–Ti, (b) 10Sn–3Cu–Ti, (c) 15Sn–3Cu–Ti, (d) 20Sn–3Cu–Ti

of divalent copper ion in pseudo-octahedral coordination suggesting the formation of segregated copper oxide particles [44], which is too small to detect by XRD patterns.

FT-IR spectra of pyridine-adsorbed for different Sn–Cu–Ti samples are shown in Fig. 6. The bands at 1455 and 1545 cm^{-1} could be assigned to the effects between pyridine and Lewis and Brønsted acid sites, respectively [45]. From Fig. 6, it can be seen that the samples mainly have Lewis acid sites and it would be promoted with the tin species increasing, which would be beneficial to their catalytic performances in the B–V oxidation of cyclohexanone by molecular oxygen.

Figure 7 is the TEM images for different Sn–Cu–Ti samples. It can be seen from Fig. 7 that the typical ordered mesostructure was obviously observed, and with the weight percent of tin species increasing, the fringe of the crystal lattice becomes more and more obscure owing to the blockage of tin species in the pores probably [29], which is coincident with the XRD pattern results. The HR-TEM images seen from Fig. 7d show that the framework of TiO_2 is crystallized with lattices in the d -spacing of 0.346 nm, which is well-matched to the 101 reflection [46]. In addition, the (111) planes for SnO_2 can be identified by the typical interfringe distance of 0.211 nm [42, 47, 48]. Meanwhile, the (020) planes for CuO can be identified by the typical interfringe distance of 0.170 nm [39, 49, 50], indicating the tin species and copper species would be homogeneously incorporated in

Fig. 7 TEM images for different Sn–Cu–Ti samples. **a** 5Sn–3Cu–Ti, **b** 10Sn–3Cu–Ti, **c** 15Sn–3Cu–Ti, **d** HR-TEM for 15Sn–3Cu–Ti sample

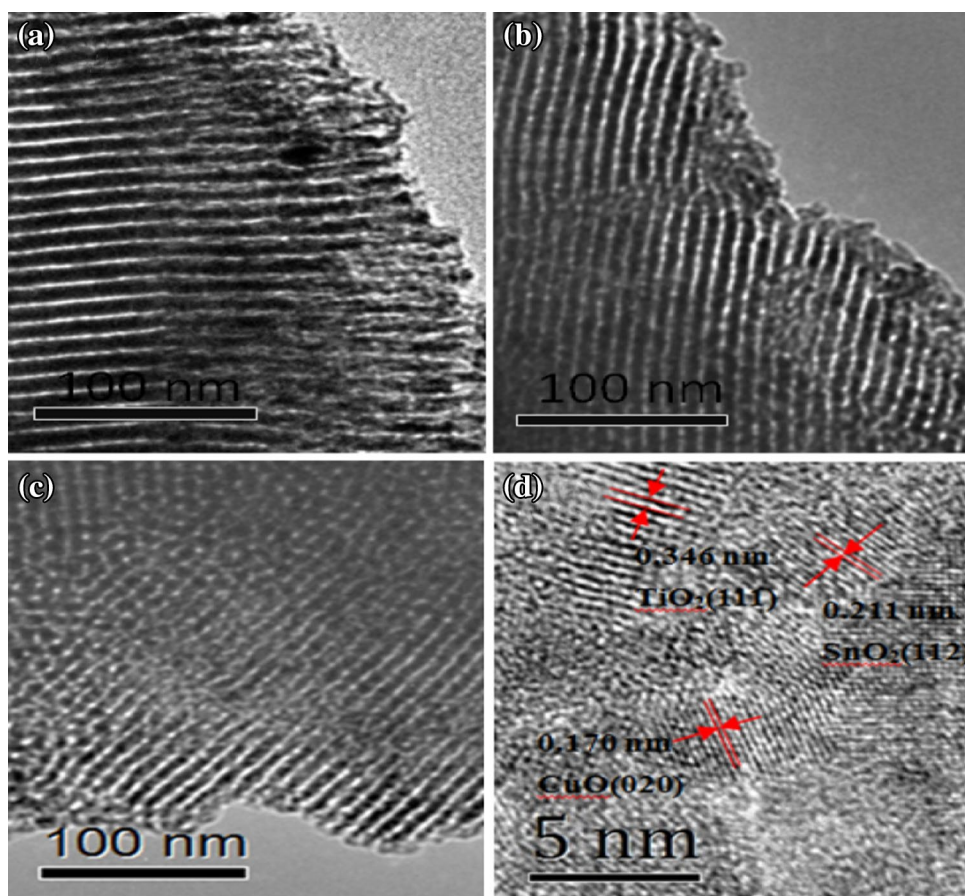
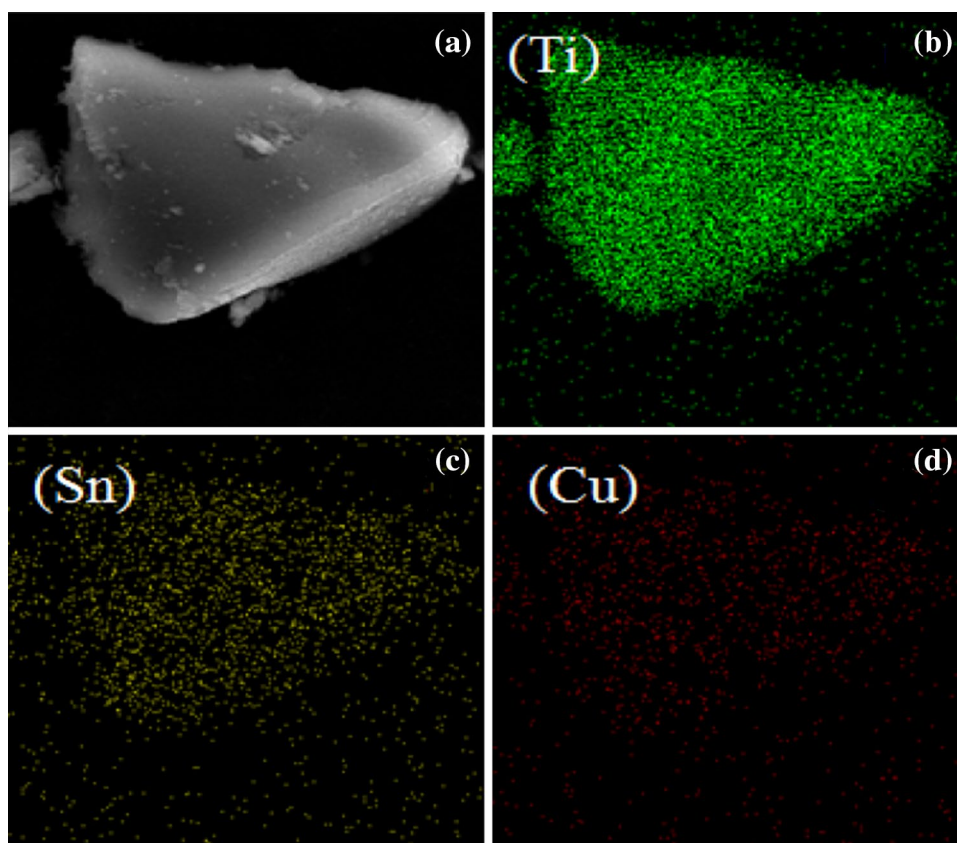


Fig. 8 SEM photo (a) and electron mapping of particles (b–d) for 15Sn–3Cu–Ti sample



the framework of anatase TiO_2 . Figure 8 was the SEM photo and electron mapping of particles for 15Sn–3Cu–Ti sample. It can be seen that the EDX element mapping showed uniform X-ray intensities of the Ti, Sn and Cu signals, suggesting their homogeneous distribution, which agrees with the XRD analysis.

3.2 Catalyst performance

The catalytic behaviors of different catalysts in the B–V oxidation of cyclohexanone by molecular oxygen are investigated and the results are listed in Table 2. From Table 2, with the tin species loading increasing from 5 to 15, cyclohexanone conversion, ϵ -caprolactone selectivity and TON value increased, and then dropped at higher tin species loading. The most active catalyst was 15Sn–3Cu–Ti, giving a cyclohexanone conversion of 96.3%, ϵ -caprolactone selectivity of 95.2% and TON value of 3.5 owing to its appropriate BET surface area and acidity, especially Lewis acid sites, which is much higher than the results of the literature [34]. However, the 15Sn–3Cu/Ti catalyst prepared by impregnation method shows only a cyclohexanone conversion of 73.1%, ϵ -caprolactone selectivity of 81.2% and TON value of 2.3, which is much lower than 15Sn–3Cu–Ti catalyst prepared by AcHE method although the tin species and copper species are the same.

Table 2 Catalytic performances for different catalysts in the B–V oxidation of cyclohexanone by molecular oxygen

Catalysts	Cyclohexanone conversion (%)	Caprolactone selectivity (%)	TON ^a
15Sn–3Cu/Ti	73.1	81.2	2.3
5Sn–3Cu–Ti	88.1	89.2	2.8
10Sn–3Cu–Ti	91.4	92.6	3.1
15Sn–3Cu–Ti	96.3	95.2	3.5
20Sn–3Cu–Ti	92.4	91.6	3.4

Reaction conditions: $w(\text{catalyst})/w(\text{cyclohexanone})=0.24$; $w(\text{acetonitrile})/w(\text{cyclohexanone})=30$; $w(\text{benzaldehyde})/w(\text{cyclohexanone})=2.4$; reaction time: 5 h; O_2 : 10 ml/min; reaction temperature: 343 K

^aTurnover number (TON): moles of product per mol of catalyst

Table 3 lists the results of the catalytic stability for 15Sn–3Cu–Ti catalyst. The conversion of cyclohexanone, selectivity of ϵ -caprolactone and TON value decreased slightly with the increase of reaction number, and cyclohexanone conversion of 88.9%, ϵ -caprolactone selectivity of 89.1% and TON value of 3.0 can be obtained after repeated reaction for 5 times, suggesting its good catalytic stability.

Table 3 Catalytic reusability for 15Sn–3Cu–Ti catalyst

Reaction number	Cyclohexanone conversion (%)	Caprolactone selectivity (%)	TON
1	96.3	95.2	3.5
2	93.5	93.2	3.4
3	90.7	91.8	3.2
4	89.6	90.6	3.1
5	88.9	89.1	3.0

Reaction conditions: $w(15\text{Sn}-3\text{Cu}-\text{Ti})/w(\text{cyclohexanone})=0.24$; $w(\text{acetonitrile})/w(\text{cyclohexanone})=30$; $w(\text{benzaldehyde})/w(\text{cyclohexanone})=2.4$; reaction time: 5 h; O_2 : 10 ml/min; reaction temperature: 343 K

4 Conclusions

The multifunctional three-component ordered mesoporous Sn–Cu–Ti samples with different tin and copper species loading were successfully prepared by AcHE method in this paper. The tin and copper species can be almost incorporated into the mesoporous framework of anatase TiO_2 and the physical chemical properties would be promoted, especially the Lewis acidity. The prepared 15Sn–3Cu–Ti catalyst shows higher catalytic performances than other samples in the B–V oxidation of cyclohexanone by molecular oxygen, and cyclohexanone conversion of 96.3%, ϵ -caprolactone selectivity of 95.2% and TON value of 3.5 can be obtained. The 15Sn–3Cu–Ti catalyst has good catalytic stability, and cyclohexanone conversion of 88.9%, ϵ -caprolactone selectivity of 89.1% and TON value of 3.0 can be obtained even after repeated reaction for 5 times.

Acknowledgements This work was supported by Jiangsu Planned Projects for Postdoctoral Research Funds (1302121C); Open Project of Beijing Key Laboratory for Enze Biomass and Fine Chemicals; Project Funded by the Priority Academic Program Development of Jiangsu Higher Education Institutions.

References

1. A. Baeyer, V. Villiger, *Ber. Deut. Bot. Ges.* **32**, 3625 (1899)
2. A. Corma, L.T. Nemeth, M. Renz, S. Valencia, *Nature* **412**, 423 (2001)
3. J.X. Li, Y.Y. Le, W.L. Dai, H.X. Li, K.N. Fan, *Catal. Commun.* **9**, 1334–1341 (2008)
4. T. Kawabata, N. Fujisaki, T. Shishido, K. Nomura, T. Sano, K. Takehira, *J. Mol. Catal. A* **253**, 279 (2006)
5. H. Subramanian, E.G. Nettleton, S. Budhi, R.T. Koodali, *J. Mol. Catal. A* **330**, 66 (2010)
6. T. Kawabata, Y. Ohishi, S. Itsuki, N. Fujisaki, T. Shishido, K. Takaki, Q. Zhang, Y. Wang, K. Takehira, *J. Mol. Catal. A* **236**, 99 (2005)
7. Y. Nabae, H. Rokubuichi, M. Mikuni, Y. Kuang, T. Hayakawa, M.A. Kakimoto, *ACS Catal.* **3**, 230 (2013)
8. S. Friess, N. Farnham, *J. Am. Chem. Soc.* **72**, 5518 (1950)
9. B. Dutta, S. Jana, S. Bhunia, H. Honda, S. Koner, *Appl. Catal. A* **382**, 90 (2010)
10. K. Kaneda, T. Yamashita, *Tetrahedron Lett.* **37**, 4555 (1996)
11. R. Llamas, C.J. Sanchidrián, J.R. Ruiz, *Tetrahedron* **63**, 1435 (2007)
12. Z.Z. Shi, C. Zhang, C.H. Tang, N. Jiao, *Chem. Soc. Rev.* **41**, 3381 (2012)
13. K. Pamin, M. Prończuk, S. Basağ, W. Kubiak, Z. Sojka, J. Połtowicz, *Inorg. Chem. Commun.* **59**, 13 (2015)
14. S. Rahman, N. Enjamuri, R. Gomes, A. Bhaumik, D. Sen, S. Mazumdar, *Appl. Catal. A* **505**, 515 (2015)
15. J. Zang, Y. Ding, L. Yan, T. Wang, Y. Lu, L. Gong, *Catal. Commun.* **51**, 24 (2014)
16. R. Kumar, P.P. Das, A.S. Al-Fatesh, A.H. Fakeeha, J.K. Pandey, B. Chowdhury, *Catal. Commun.* **74**, 80 (2015)
17. S.Y. Chen, X.T. Zhou, H.B. Ji, *Catal. Today* **264**, 191 (2015)
18. D.Y. Zhao, J.L. Feng, Q.S. Huo, N. Melosh, G.H. Fredrickson, B.F. Chmelka, G.D. Stucky, *Science* **279**, 548 (1998)
19. J. Liu, S.Z. Qiao, Q.H. Hu, G.Q. Lu, *Small* **7**, 425 (2011)
20. W. Teng, Z. Wu, J. Fan, H. Chen, D. Feng, Y. Lv, J. Wang, A.M. Asiri, D. Zhao, *Energy. Environ. Sci.* **6**, 2765 (2013)
21. X.H. Sun, Y.F. Shi, P. Zhang, C.M. Zheng, X.Y. Zheng, F. Zhang, Y.C. Zhang, N.J. Guan, D.Y. Zhao, G.D. Stucky, *J. Am. Chem. Soc.* **133**, 14542 (2011)
22. F.X. Wang, L. Liang, J. Ma, L. Shi, J.M. Sun, *Eur. J. Inorg. Chem.* **18**, 2934 (2014)
23. P. Doggali, Y. Teraoka, P. Mungse, I.K. Shah, S. Rayalu, N. Labhsetwar, *J. Mol. Catal. A* **358**, 23 (2012)
24. H.X. Li, Z.F. Bian, J. Zhu, D.Q. Zhang, G.S. Li, Y.N. Huo, H. Li, Y.F. Lu, *J. Am. Chem. Soc.* **129**, 8406 (2007)
25. A. Kojima, K. Teshima, Y. Shirai, T. Miyasaka, *J. Am. Chem. Soc.* **131**, 6050 (2009)
26. T. Takeguchi, O. Takeoh, S. Aoyama, J. Ueda, R. Kikuchi, K. Eguchi, *Appl. Catal. A* **252**, 205 (2003)
27. X. Wang, R.J. Gorte, J.P. Wagner, *J. Catal.* **212**, 225 (2002)
28. Z.W. Zhou, Y. Yu, P.C. Yu, J. Qin, S.S. Dai, W.L. Wu, *React. Kinet. Mech. Catal.* **120**, 295 (2017)
29. Z.W. Zhou, P.C. Yu, J. Qin, W.L. Wu, X. Lin, Z.Q. Gu, X.Q. Liu, *J. Porous Mater.* **23**, 239–245 (2016)
30. Y. Yoon, R.K. Bo, Y.L. Chang, J. Kim, *Asian J. Org. Chem.* **5**, 746 (2016)
31. W. Zhou, Y. Chen, J. Qian, F. Sun, M. He, Q. Chen, *Catal. Lett.* **146**, 2157 (2016)
32. S.E. Allen, R.R. Walvoord, R. Padilla-Salinas, M.C. Kozłowski, *Chem. Rev.* **113**, 6234 (2013)
33. T. Punniyamurthy, L. Rout, *Coord. Chem. Rev.* **252**, 34 (2008)
34. H.F. Huo, L. Wu, J.X. Ma, H.L. Yang, L. Zhang, Y.Y. Yang, S.W. Li, R. Li, *ChemCatChem* **8**, 779 (2016)
35. D.H. Pan, M. Guo, M. He, S.W. Chen, X. Wang, F. Yu, R.F. Li, *J. Mater. Res.* **29**, 811 (2014)
36. H. Meng, L.P. Yuan, J.J. Gao, N.N. Ren, Y.Z. Lu, C.X. Li, *RSC Adv.* **7**(17), 10407 (2017)
37. J. Fan, Y.H. Dai, Y.L. Li, N.F. Zheng, J.F. Guo, X.Q. Yan, G.D. Stucky, *J. Am. Chem. Soc.* **131**(43), 15568 (2009)
38. Z.C. Miao, H.H. Zhao, J. Yang, J. Zhao, H.L. Song, L.J. Chou, *Microporous Mesoporous Mater.* **198**, 271 (2014)
39. H.Y. Min, X.Q. Ran, J.W. Fan, Y. Su, J.P. Yang, W. Teng, W.X. Zhang, G.M. Li, D.Y. Zhao, *J. Mater. Chem. A* **3**, 7399 (2015)
40. L. Lopez, V. Montes, H. Kusar, S. Cabrera, M. Boutonnet, S. Jaras, *Appl. Catal. A* **526**, 77 (2016)
41. A.C. Pradhan, K.M. Parida, *J. Mater. Chem.* **22**(15), 7567 (2012)
42. M.J. Chen, J.P. Yang, Y. Liu, D.Y. Zhao, *J. Mater. Chem. A* **3**, 1405 (2015)
43. A.W. Xu, Y. Gao, H.Q. Liu, *J. Catal.* **207**, 151 (2002)

44. N. Brodie-Linder, R. Besse, F. Audonnet, S. LeCaer, J. Deschamps, M. Impéror-Clerc, C. Alba-Simionesco, *Microporous Mesoporous Mater.* **132**, 518 (2010)
45. Q. Zhang, H.H. Yang, W. Yan, *RSC Adv.* **4**, 56938 (2014)
46. C.L. Wang, J.Y. Liao, Y.B. Zhao, A. Manthiram, *Chem. Commun.* **51**, 2848 (2015)
47. G.E. Cheng, J.Y. Chen, H.Z. Ke, J. Shang, R. Rui, *Mater. Lett.* **65**(21), 3327 (2011)
48. X.H. Ding, D.W. Zeng, C.S. Xie, *Sens. Actuators B* **149**, 336 (2010)
49. C. Tamuly, M. Hazarika, J. Das, M. Bordoloi, D.J. Borah, M.R. Das, *Mater. Lett.* **123**, 202 (2014)
50. H.R. Kim, T. Ito, B.S. Kim, I.S. Kim, *J. Exp. Nanosci.* **8**, 852 (2013)